PAGEOPH, Vol. 128, Nos. 1/2 (1988) 0033-4553/88/020401-21$1.50 + 0.20/0

Linearized Rays, Amplitude and Inversion

ROBERT L. NOWACK[1] and WILLIAM J. LUTTER[1]

Abstract—In this paper, ray theoretical amplitudes and travel times are calculated in slightly perturbed velocity models using perturbation analysis. Also, test inversions using travel time and amplitude are computed. The perturbation method is tested using a 3-D velocity model for NORSAR having velocity variations up to 8.0 percent. The perturbed amplitudes are found to be in excellent agreement with the calculated ray amplitudes. Velocity inversions based on travel time and amplitude are next investigated. Perturbation analysis using linearized ray equations is efficiently used to compute amplitude derivatives with respect to model parameters. The trial linearized inversions use smaller velocity variations of 1.7 percent to avoid possible effects due to ray shift, even though the perturbation analysis is valid for larger variations. The trial 2-D inversion results show that linearized amplitude inversions are complementary and not redundant to travel time inversions, even in smoothly varying models.

Key words: Linearized inversion, ray theory, amplitude variations.

Introduction

In this paper, ray theoretical amplitudes and travel times are computed in slightly perturbed velocity models using perturbation analysis. Test results using velocity models for NORSAR indicate that rays calculated in one model can be used to calculate travel times and amplitudes in perturbed models with velocity variations up to 8 percent different from the original model. One application of this approach is to the calculation of ray theoretical results in complicated 3-D models using ray tracing in simpler, say 1-D, velocity models. This approach can also be applied to the calculation of Gaussian beam and Maslov synthetic seismograms in slightly perturbed velocity models.

Velocity inversions based on ray theoretical amplitude and travel time, are next investigated. Recent inversion results by NOWACK and AKI (1986) indicate possible limitations using a linearized waveform analysis for large scale velocity anomalies. A Rytov linearization was suggested to extend the linear region. Another approach

[1] Department of Earth and Atmospheric Sciences, Purdue University, West Lafayette, IN 47907, U.S.A.

is to extend travel time inversions using ray theoretical amplitudes. Perturbation analysis can be efficiently used to compute amplitude derivatives with respect to model parameters. In the trial linearized inversion examples, only smaller variations of 1.7 percent are used to avoid possible nonlinear effects due to ray shift, even though the perturbation approach is valid for larger variations. Trial results indicate that linearized inversions based on travel time and ray amplitude are complementary and not redundant even using the same smooth model. Amplitudes appear to resolve the edges of heterogeneities. Linearized amplitude inversions may therefore not necessarily predict travel times, being sensitive to different features of the model.

1. Linearized Ray Equations

In this section, the ray equations are presented in different coordinate systems and then linearized to give the dynamic ray equations. In an isotropic medium, the ray equations can be written

$$\frac{dx_i}{ds} = H_{,p_i} = u^{-1}(\underline{x})p_i$$

$$\frac{dp_i}{ds} = -H_{,x_i} = \frac{\partial}{\partial x_i} u(\underline{x})$$

where $i = 1, 3$, $\underline{p}$ is the slowness vector tangent to ray, $\underline{x}$ is the position vector along ray, and $u(\underline{x})$ is the slowness along the ray. These equations are subject to the constraint $p_i p_i = u^2(x)$. The Hamiltonian for this system can be written

$$H = \frac{u^{-1}(x)}{2}(p_i p_i - u^2(\underline{x})).$$

The first step in deriving linearized ray equations is to rewrite the ray equations with respect to a preferred axis, say x_3 (see Figure 1a). In 3-D this reduces the number of equations from 6 to 4. The reduced ray equations can also be written in an orthogonal curvilinear coordinate system about a known reference ray instead of the x_3 axis (see POPOV and PŠENČÍK, 1976, 1978). The reduced ray equations in 'ray centered' coordinates are shown in Figure 1b, and are written

$$\frac{dq_I}{dq_3} = H_{,p_I}$$

$$\frac{dp_I}{dq_3} = -H_{,q_I}$$

where $I = 1, 2$. The Hamiltonian can now be written

$$H = -p_3 = -h_3(u^2(\underline{x}) - h_I^{-2} p_I p_I)^{1/2}$$

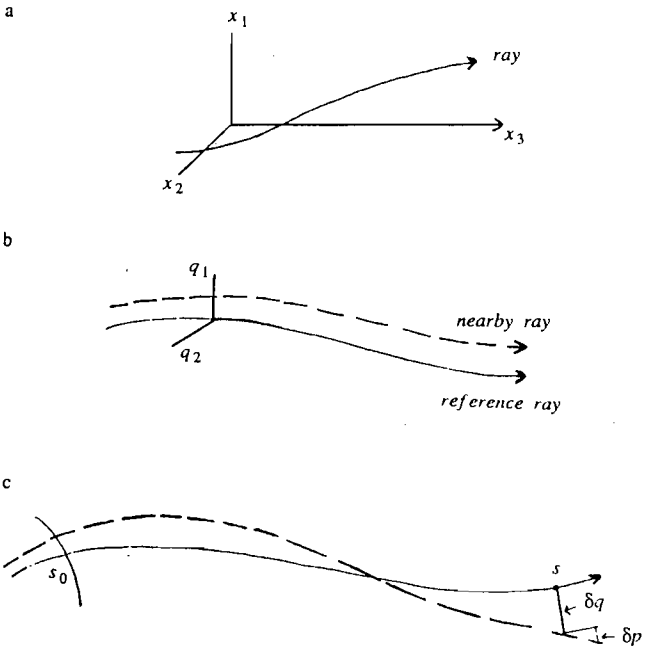

Figure 1
a) Reduced ray equations can be written with respect to a preferred direction, x_3. b) Reduced ray equations can be also written in ray centered coordinates. c) In ray centered coordinates, the reduced ray equations can be linearized near the reference ray giving the dynamic ray equations.

where the scale factors are

$$h_1 = h_2 = 1 \quad h_3 = 1 - u^{-1}u_{,q_I}q_I.$$

All functions are evaluated along central reference ray at $q_I = 0$.

For rays nearby the reference ray, the reduced ray equations in 'ray centered' coordinates can be linearized by expanding H nearby the reference ray

$$H_{,p} \approx [H_0 + H_{,q}\delta q + H_{,p}\delta p]_{,p}$$

$$H_{,q} \approx [H_0 + H_{,q}\delta q + H_{,p}\delta p]_{,q}$$

where δq and δp are the perturbations of the position and slowness vector of the nearby ray in ray centered coordinates about the reference ray (see Figure 1c). This results in the dynamic ray equations which are linearized paraxial equations in ray centered coordinates. The dynamic ray equation can be written

$$\frac{d}{ds}\begin{bmatrix}\delta q \\ \delta p\end{bmatrix} = A\begin{bmatrix}\delta q \\ \delta p\end{bmatrix} \tag{1}$$

where δq and δp are position change and slowness change vectors of length 2. A is

a 4×4 matrix of the form

$$A = \begin{bmatrix} H_{qp} & H_{pp} \\ -H_{qq} & -H_{pq} \end{bmatrix} = \begin{bmatrix} 0 & u^{-1}I \\ u_{qiqj} - 2u^{-1}u_{qi}u_{qj} & 0 \end{bmatrix}$$

where u is the slowness along the reference ray and u_q and u_{qq} are the first and second derivatives evaluated along the reference ray. The dynamic ray equations in the ray-centered coordinates are similar to the paraxial ray equations in a Cartesian x_3 oriented system.

The linear dynamic ray equations can be solved using the propagator $P(s, s_0)$ for this system of equations. Any solution, $(\delta q, \delta p)$, can be written in terms of the propagator and the initial conditions as

$$\begin{bmatrix} \delta q \\ \delta p \end{bmatrix} = P(s, s_0) \begin{bmatrix} \delta q_0 \\ \delta p_0 \end{bmatrix}.$$

Once $P(s, s_0)$ is calculated, the entire set of nearby rays can be found by adjusting the initial conditions. A fundamental application of the propagator formulation of the dynamic ray equations is to 2-point ray tracing (see ČERVENÝ *et al.*, 1984, 1987; CORMIER and BEROZA, 1987). A second important application of the dynamic ray equations is in the calculation of spreading amplitudes. From the transport equation, ray amplitude is related to the geometric spreading by an inverse square root, $A \approx J^{-1/2}$. From the geometry of ray tube spreading near a given ray, the amplitude can be obtained from the ray propagator

$$P(s, s_0) = \begin{bmatrix} Q_1 & Q_2 \\ P_1 & P_2 \end{bmatrix}.$$

In the 3-D case, each sub-matrix of the propagator is a 2×2 matrix. For an initial 3-D point source, $J = \det Q_2 / v^2(s_0)$, where $v(s_0)$ is the initial velocity, and for an initial plane wave, $J = \det Q_1$. Thus spreading amplitude can be obtained from the linearized dynamic ray equations (see ČERVENÝ and HRON, 1980).

2. *Ray Theoretical Seismograms in Perturbed Velocity Models*

The calculation of ray theoretical amplitudes and travel times in slightly perturbed velocity models is investigated in this section. The perturbation theory of FARRA and MADARIAGA (1987) has been followed. This approach allows for the use of simple structures in order to compute ray theoretical results in more complicated models by perturbation, without additional ray tracing.

The first-order perturbation of travel time with respect to slowness can be written

$$\delta T = \frac{\partial T}{\partial u} \delta u = \int_{s_0}^{s} \delta u(\underline{x})\, ds.$$

Thus, the travel time perturbation due to slowness variations can to first order be computed by integrating the slowness perturbations along the original ray trajectory in the unperturbed medium. This has been used successfully for the efficient calculation of sensitivity operators in seismic travel time tomography studies (see AKI *et al.*, 1976; AKI, 1977; CLAYTON and COMER, 1983; DZIEWONSKI, 1984).

In contrast, for amplitudes a perturbation of the reference ray may be required. The reference ray perturbation is solved by a linearized set of ray equations similar to the dynamic ray equations except for a source term involving the perturbed material slowness parameters. First, the Hamiltonian, H, is expanded to first order in changes of the reference ray by a material slowness perturbation along the path (see FARRA and MADARIAGA, 1987)

$$H = H_0 + H_{,q}\delta q_r + H_{,p}\delta p_r + \frac{\partial H}{\partial u}\delta u.$$

This results in an inhomogeneous set of linearized ray equations for the perturbation of the reference ray, $(\delta q_r, \delta p_r)$.

$$\frac{d}{ds}\begin{bmatrix}\delta q_r \\ \delta p_r\end{bmatrix} = A\begin{bmatrix}\delta q_r \\ \delta p_r\end{bmatrix} + \delta B$$

where

$$\delta B = \begin{bmatrix} 0 \\ \delta u_{q_I} - u^{-1}u_{q_I}\delta u \end{bmatrix}.$$

The source term δB results from both perturbations of the slowness, δu, and its first derivatives, δu_q. The solution can be written using an inhomogeneous propagator formulation

$$\begin{bmatrix}\delta q_r \\ \delta p_r\end{bmatrix} = \int_{s_0}^{s} P(s, s')\delta B(s')\, ds'. \tag{2}$$

As an example, the 3-D velocity model for NORSAR derived from a travel time inversion by THOMSON and GUBBINS (1982) is used (see also THOMSON, 1983). The velocity model is shown in Figure 2. Cubes are fast velocities and small spheres are slow velocities, with the size of the symbol representing the size of the heterogeneity, up to 8%. We take an east-west vertical cross-section through the center of the model and compute vertically incident rays through this structure. The ray-field is shown in Figure 3a with focusing and defocusing apparent. Figure 3b shows the ray-field derived by perturbation of the rays in Figure 3a using the formulation above in order to simulate rays in a homogeneous medium. This formulation has effectively unbent the ray-field without additional ray tracing in the final medium.

In order to compute the amplitude perturbation from a change in material

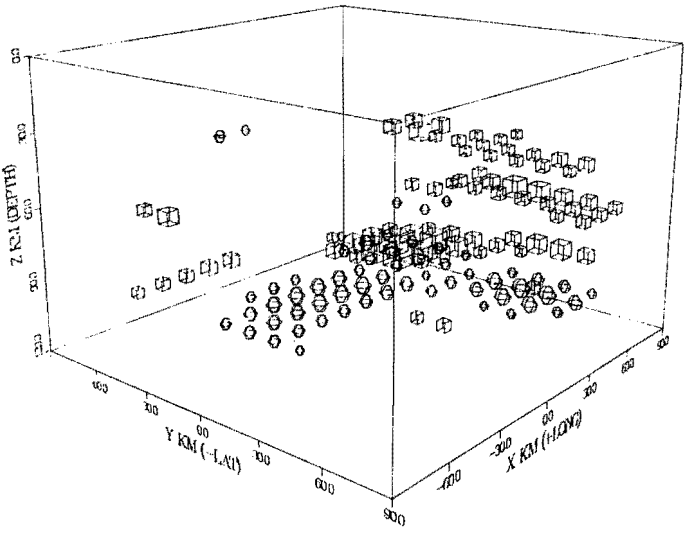

Figure 2
Velocity model for NORSAR derived by THOMPSON and GUBBINS (1982). Spheres are slow velocities and cubes are fast velocities with the size of the symbol representing the size of the heterogeneity up to 8%.

slowness/velocity, the first order perturbation to the propagator must be derived. The linearized dynamic ray equations in the perturbed medium can be written

$$\frac{d}{ds}\begin{bmatrix}\delta q\\ dp\end{bmatrix} = (A_0 + \delta A)\begin{bmatrix}\delta q\\ \delta p\end{bmatrix}.$$

The propagator in the perturbed medium also solves this equation and can be written in terms of the propagator of the unperturbed medium as $P_0 + \delta P$. To first order $\delta A \approx \delta A_1 + \delta A_2(q_r, p_r)$, where

$$\delta A_1 = \begin{bmatrix}\delta H_{pq} & \delta H_{pp}\\ -\delta H_{qq} & -\delta H_{pq}\end{bmatrix} = \begin{bmatrix}0 & -u^{-2}\delta u_l\\ \delta u_{q_l q_j} - u^{-1}(u_{q_l}\delta u_{q_j} + u_{q_j}\delta u_{q_l}) & 0\end{bmatrix}$$

and $\delta A_2(q_r, p_r)$ contains corrections due to changes in the ray trajectory (see FARRA and MADARIAGA, 1987). Introducing the propagator, $P = P_0 + \delta P$, in the above equation and neglecting the second order terms $\delta P \delta A$, a Born approximation, results in another set of inhomogeneous linearized ray equations in the unperturbed medium. The solution for the perturbed propagator can be written

$$P(s, s_0) = P_0(s, s_0) + \delta P(s, s_0) = P_0(s, s_0) + \int_{s_0}^{s} P_0(s, s')\delta A(s')P_0(s', s_0)\, ds'. \qquad (3)$$

Determinants of the upper sub-matrices of $P(s, s_0)$ give the approximate spreadings in the perturbed medium.

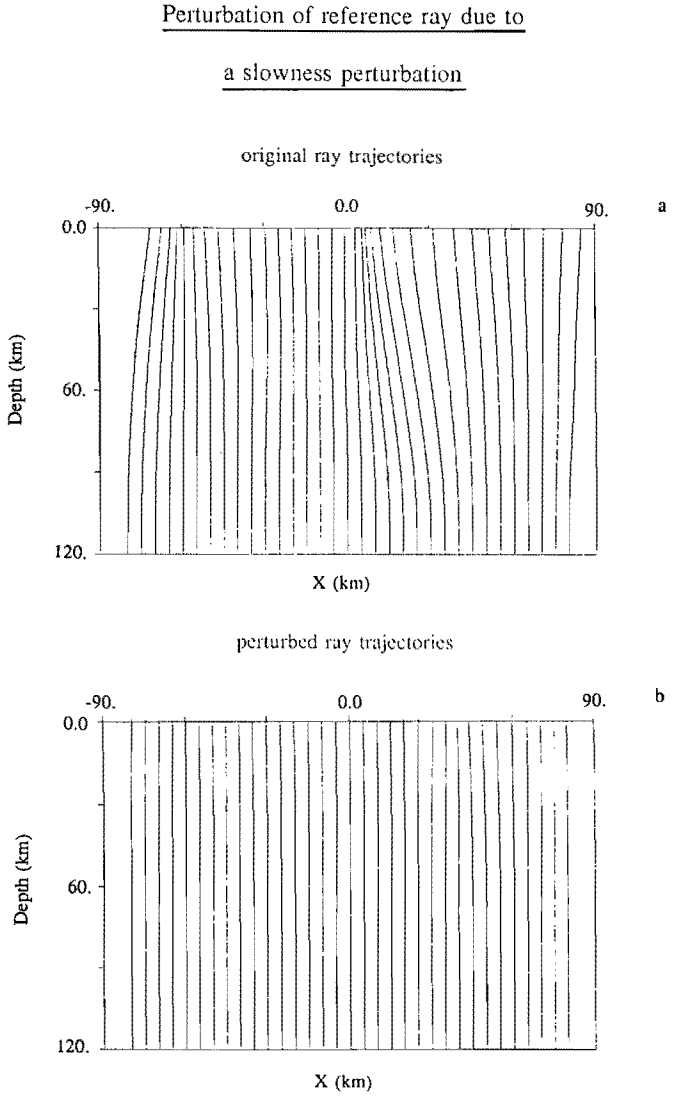

Figure 3

a) Rays traced from a vertical plane wave for an east-west vertical cross-section of the NORSAR model in Figure 2. b) Rays for an equivalent homogeneous model derived by linear perturbation of the ray trajectories in a).

Using the same cross-section of the NORSAR model as before, the geometric spreading, $J = \det Q_1$, for a vertically incident plane-wave for receivers at the surface is shown in Figure 4a. From the transport equation, the amplitude is proportional to the inverse square root of the spreading, J. The result of using the above formulation for the spreading in an equivalent homogeneous medium is

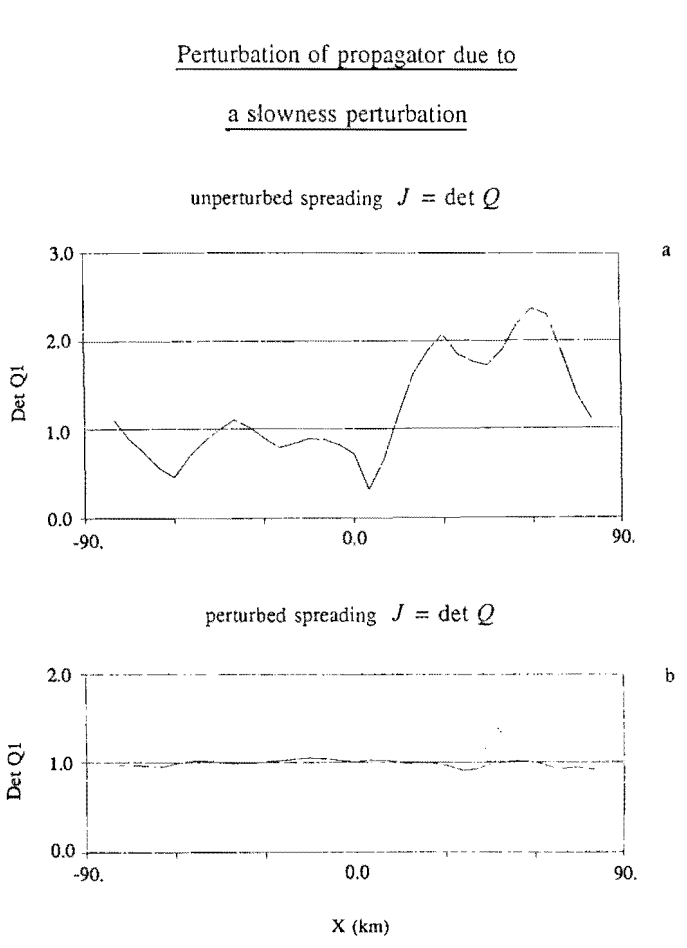

Figure 4

a) The spreading, $J = \det Q_1$, recorded on the surface for the incident plane wave shown in Figure 3a. b) The spreading for a homogeneous model derived by linear perturbation from the results in a).

shown in Figure 4b. The exact solution for a homogeneous medium has a uniform spreading of one for an incident plane-wave. The perturbation solution has come within 2% of the correct solution, using a starting model with up to 8% slowness/velocity variations.

An important application of this approach is for the use of simple velocity structures, such as 1-D models, to compute, by perturbational analysis, ray theoretical amplitude and travel time in more complicated 3-D velocity models. This approach could also be used for slightly anisotropic models where all ray tracing is performed in a nearby isotropic model (see ČERVENÝ and FIRBAS, 1984).

3. Ray Theoretical Seismic Inversion

In the following section, seismic inversions based on ray theoretical travel times and amplitudes are investigated. Waveform inversion results of NOWACK and AKI (1986) have indicated possible limitations using waveforms for large scale velocity anomalies. A Rytov linearization was suggested to extend the domain of linearity. A second approach is the extension of travel time inversions using ray theoretical amplitudes. The perturbation analysis of the previous section can be efficiently used to compute ray amplitude partial derivatives with respect to material slowness. This can then be used in amplitude and travel time inversions for slowness/velocity.

Ray theoretical amplitude can be written as $A \approx CJ^{-1/2}$, where J is the geometric spreading. The factor C can be written as a series of factors, $C = C_0C_1C_2C_3$, where C_0 gives a source amplitude, C_1 is the square root of the ratio of impedance at the layer interfaces, C_2 is the multiplicative series of plane-wave reflection and transmission coefficients, and C_3 is an intrinsic attenuation operator along the ray of the form $C_3 \approx e^{-\int \alpha(x)\, ds}$. For a more complete derivation of ray theoretical amplitudes in a heterogeneous laterally varying layered medium see ČERVENÝ (1985a).

The log-amplitude sensitivity operator due to a perturbation in material slowness is

$$\frac{\partial \ln A}{\partial u} = \frac{1}{C}\frac{\partial C}{\partial u} - 1/2J^{-1}\frac{\partial J}{\partial u}$$

where the factor, $\partial J/\partial u$, can be obtained from the perturbed propagator. Advantages of log variables include the reduction of multiplicative scaling and the conversion of a multiplicative noise structure to an additive noise structure more appropriate for least squares inversion.

The trial models to be used in the following examples are 2-D, have no interfaces, and are smoothly interpolated by splines. The models are 140 km on a side and have a 5 km node spacing. Figure 5 shows rays for a source at the bottom of the model and receivers at the top. This model has several heterogeneities with a 4% velocity contrast from a 6 km/sec background. The rays are computed using the 2-D seismic package, SEIS83 (see ČERVENÝ and PŠENČÍK, 1984). The rays are seen to be focused and bent by the heterogeneities.

Figure 6 shows the spreading, J, for receivers at the surface and a vertically incident plane-wave. A single node point of the model at $x = 70$ km, $z = 55$ km has been perturbed by 0.1 km/sec. The solid line is from an exact ray tracing calculation. The dotted line is derived from a first order perturbation of the propagator from an initial homogeneous model using Eq. (3) with the δA_1 term only. The dash-dot line is the corrected result from a first order ray shift due ray bending using Eq. (2). The remaining differences can be further reduced by incorporating the δA_2 term in Eq. (3). For the following only small perturbations from the

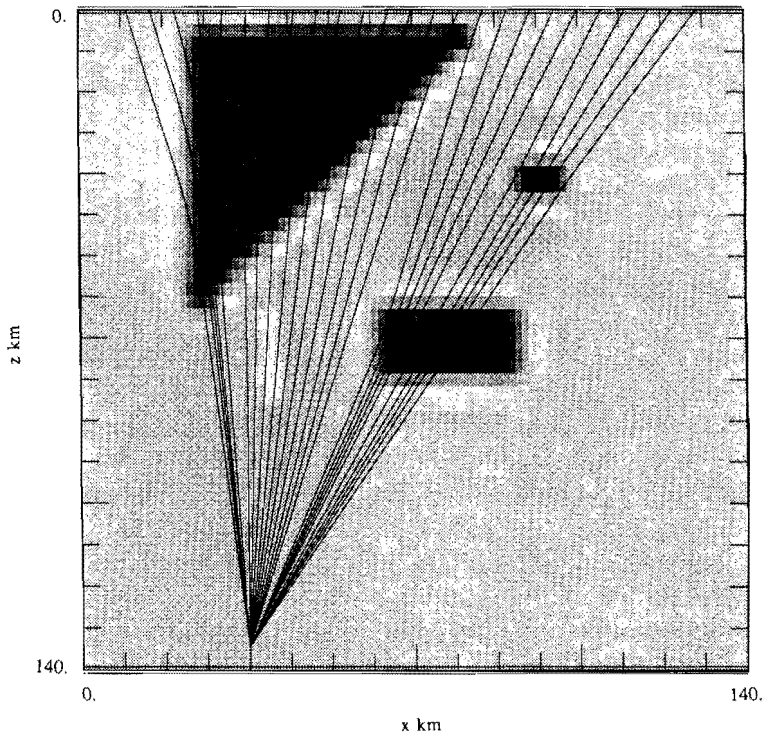

Figure 5
Rays for a source at the bottom of a smoothly varying splined trial model with receivers along the top.

reference model are required in the calculation of spreading sensitivity operators. Thus for this application, only propagator perturbations from Eq. (3) are used. For more general calculations of spreading in perturbed velocity models both the perturbation of the propagator, in Eq. (3), and the first order ray bending, in Eq. (2), must be accounted for.

In the following examples, a linearized inverse problem is solved with the form

$$\begin{bmatrix} G/\sigma_d \\ \varepsilon_1 I \\ \varepsilon_2 \nabla^2 \end{bmatrix} \delta u \approx \begin{bmatrix} d/\sigma_d \\ 0 \\ 0 \end{bmatrix} \tag{4}$$

where δu is the vector of material slowness variations to be estimated, d is the data residual vector, and G is a sparse linearized sensitivity operator. σ_d is the estimated data variance used to normalize the $G\delta u \approx d$ rows. For the travel time problem, $G = G^T = \partial T/\partial u$ and $d = T^{\text{obs}} - T^{\text{calc}}$. For the amplitude problem,

$$G = G^{\ln A} = \frac{\partial \ln A}{\partial u} = \frac{1}{A}\frac{\partial A}{\partial u}$$

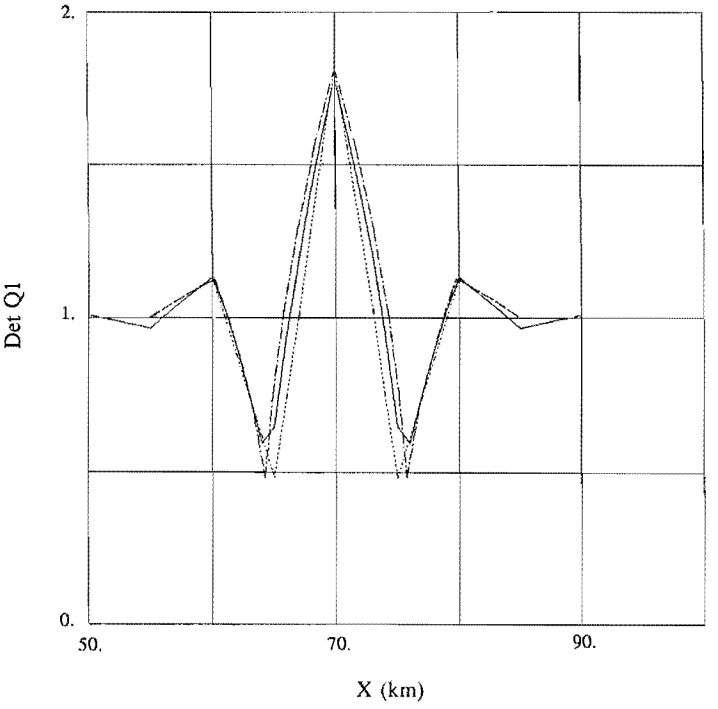

Figure 6
The spreading, $J = \det Q_1$, for a vertically incident plane wave. The solid line is the exact ray spreading, for single node of the model at $x = 70$ km, $z = 55$ km perturbed by 0.1 km/sec from a 6.0 km/sec background. The dotted line is the result of linear perturbation of the propagator in Eq. (3). The dash-dot line corrects for the ray shift in Eq. (2).

and $d = \ln[A^{\text{obs}}/A^{\text{calc}}]$. In the following, just the spreading part of the amplitude partial, $\partial J/\partial u$, will be used.

The system is stabilized first by a dampening parameter, ε_1, which controls the influence of the equations $\delta u \approx 0$, and reduces the effect of small singular values on the solution. In terms of a stochastic inverse formulation, ε_1 is proportional to the inverse square root of the *a priori* model variance, thus $\varepsilon_1 \approx \sigma_u^{-1}$ (see AKI and RICHARDS, 1980). The parameter ε_2 controls the smoothness of the solution by weighting the equations, $\nabla^2(\delta u) \approx 0$.

In order to take advantage of the sparseness of Eq. (4), the Paige-Saunders conjugate-gradient algorithm is used to solve both the travel time and amplitude problems (see PAIGE and SAUNDERS, 1982a, 1982b; NOLET, 1985; LUENBERGER, 1984). This is an iterative algorithm which solves the linearized matrix equation and does not require explicit matrix inversion. In addition, it only requires storage of the nonzero matrix elements. In the typical cases to be shown with 361 unknowns, 200 to 300 iterations were required to reach single precision machine tolerances

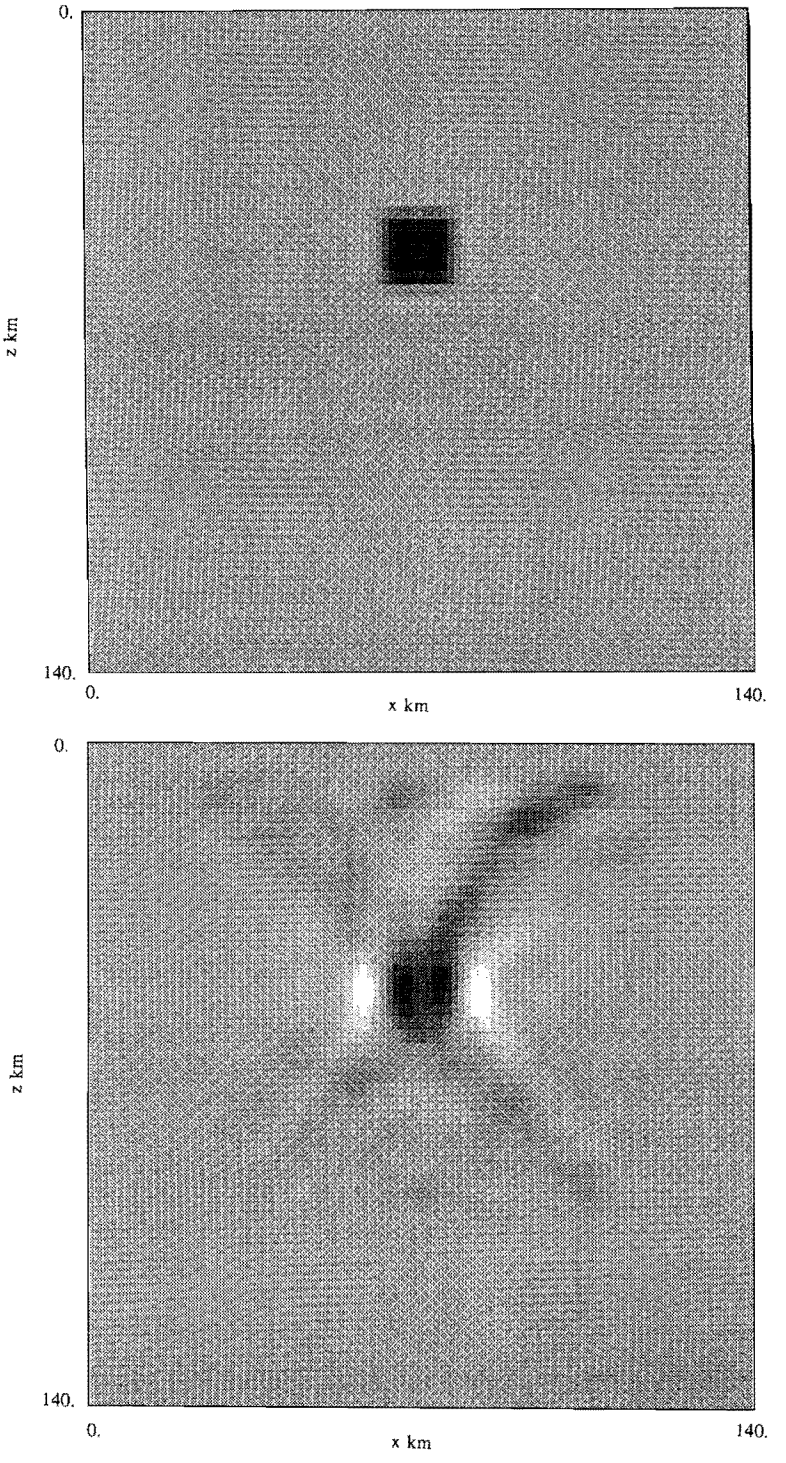

Figure 7(a,b)

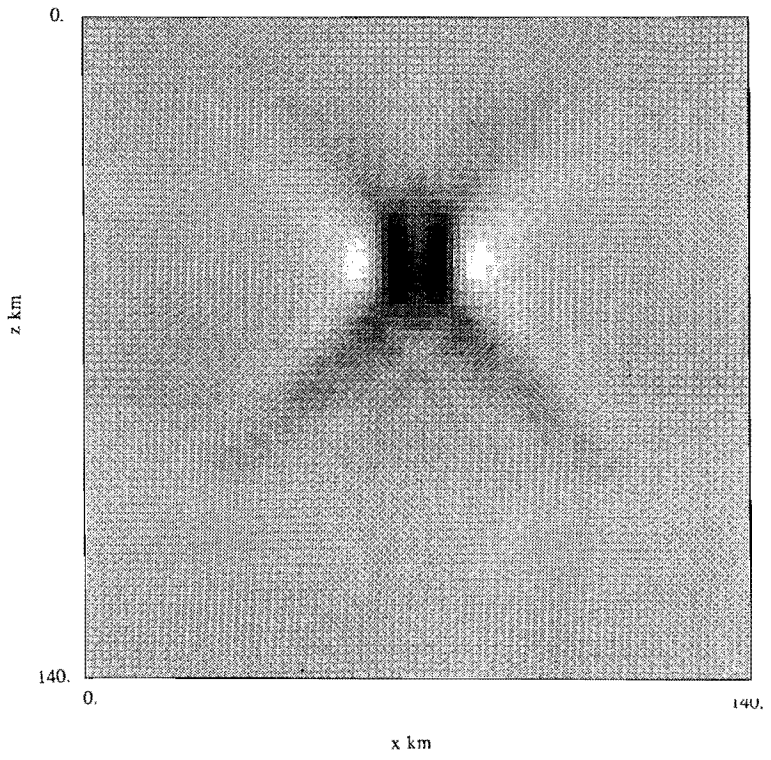

Figure 7
a) Trial model with small heterogeneity with a contrast of 0.1 km/sec above a 6.0 km/sec background. Shading ranges from 5.95 to 6.14 km/sec. b) Travel time inversion for sources below and receivers along the top. Damping and smoothing parameters are $\varepsilon_1 = 10$ and $\varepsilon_2 = 5$. Shading ranges from 5.96 to 6.11 km/sec b) and c). c) Amplitude inversion with damping and smoothing parameters, $\varepsilon_1 = 4$ and $\varepsilon_2 = 2$.

recommended by PAIGE and SAUNDERS (1982b), taking about 10 minutes on a Sun 3/50 workstation. The maximum allowable number of iterations was set to twice the number of unknowns. This is much faster than equivalent normal equation or singular value inversions making larger problems feasible. The conjugate gradient algorithm was compared with a normal equations approach using a smaller test model of 15 unknowns and good agreement was found.

The trial models to be used are smoothly interpolated by splines with no interfaces. 25 receivers are placed on the upper surface and 15 sources along the bottom of the model giving 375 travel time or amplitude observations. The central section of the model is divided into 361 blocks resulting in an only slightly overdetermined inversion problem.

In Figure 7a, a single small scale heterogeneity is illuminated by sources from below. The velocity contrast is 0.1 km/sec above a 6.0 km/sec background. This gives a 1.7% velocity anomaly. The reason for using a smaller magnitude anomaly

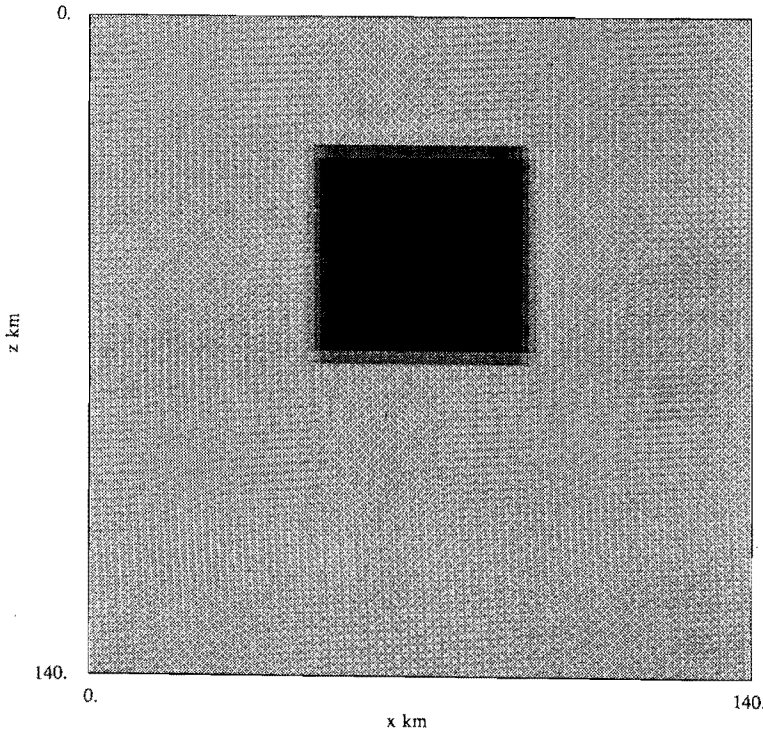

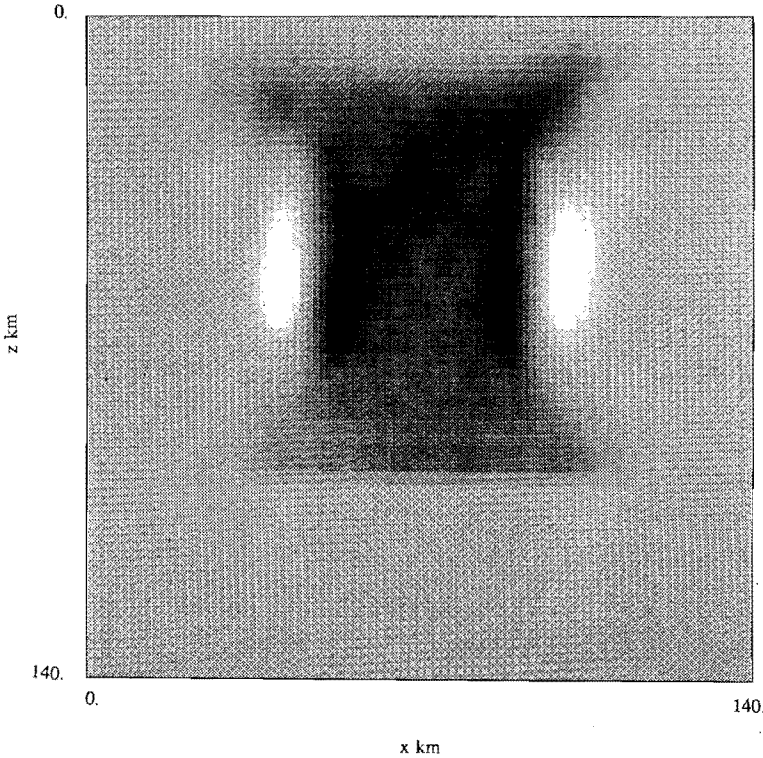

Figure 8(a,b)

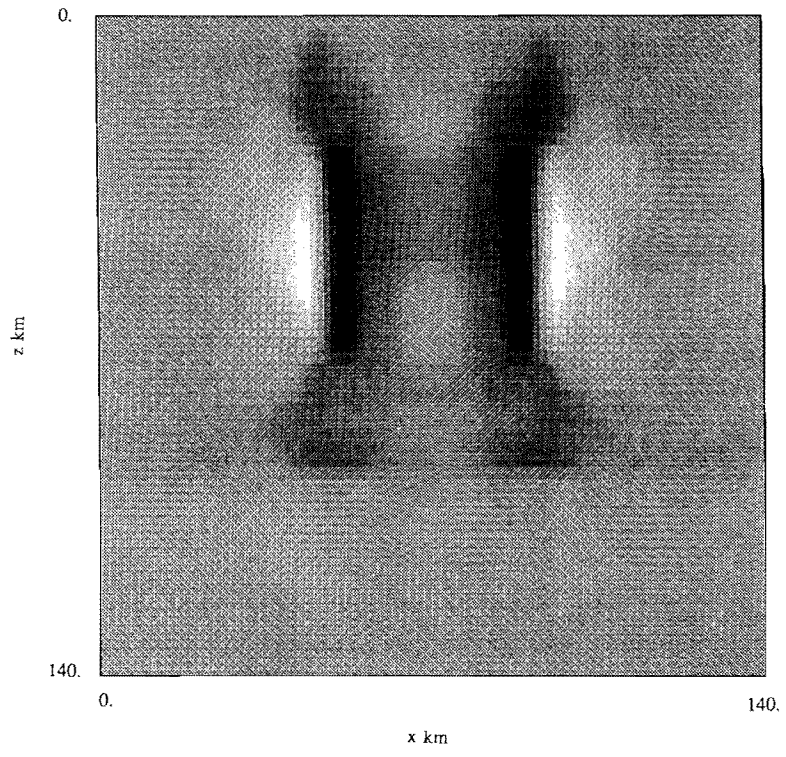

Figure 8

a) Trial model with larger heterogeneity with a contrast of 0.1 km/sec above a 6.0 km/sec background. Shading ranges from 5.95 to 6.14 km/sec. b) Travel time inversion with $\varepsilon_1 = 10$ and $\varepsilon_2 = 5$. Shading ranges from 5.96 to 6.11 km/sec for b) and c). c) Amplitude inversion with $\varepsilon_1 = 4$ and $\varepsilon_2 = 2$.

for the trial velocity inversions is to initially avoid any problems due to ray shift, however the perturbation approach is valid for larger variations. The travel time inversion for this case is shown in Figure 7b with $\varepsilon_1 = 10$ and $\varepsilon_2 = 5$. The value of ε_2 is chosen to reduce adjacent block fluctuations and smooth the image. The object is reasonably well reconstructed with side lobes and vertical elongation due to the ray geometry. Figure 7c shows the result of an inversion based on the amplitude information with ε_1 equal to 4 and ε_2 equal to 2. The object is sharper than in the travel time case but vertical elongation is still apparent. Both the linearized travel time and amplitude results for this case recover a significant fraction of the magnitude of the anomaly.

In Figure 8a, a larger heterogeneity is used, again interpolated by splines. The velocity contrast is again 0.1 km/sec above a 6.0 km/sec background. Figure 8b shows the results of a travel time inversion with $\varepsilon_1 = 10$ and $\varepsilon_2 = 5$. Note that the inverted object has poor vertical resolution due to the ray geometry. Figure 8c shows an amplitude inversion for the same model with $\varepsilon_1 = 4$ and $\varepsilon_2 = 2$. The first observation is that the amplitude inversion appears to extract the vertical edges of

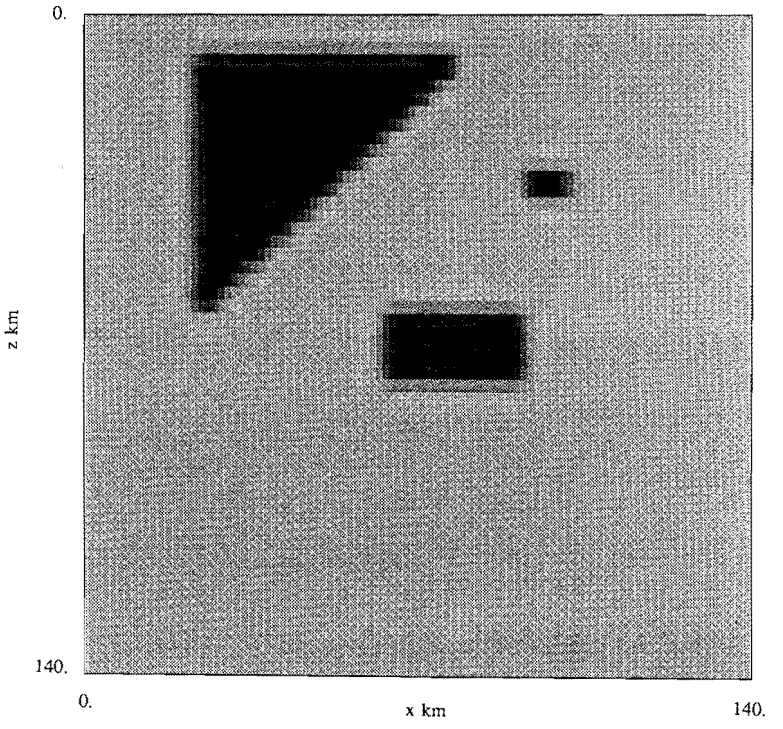

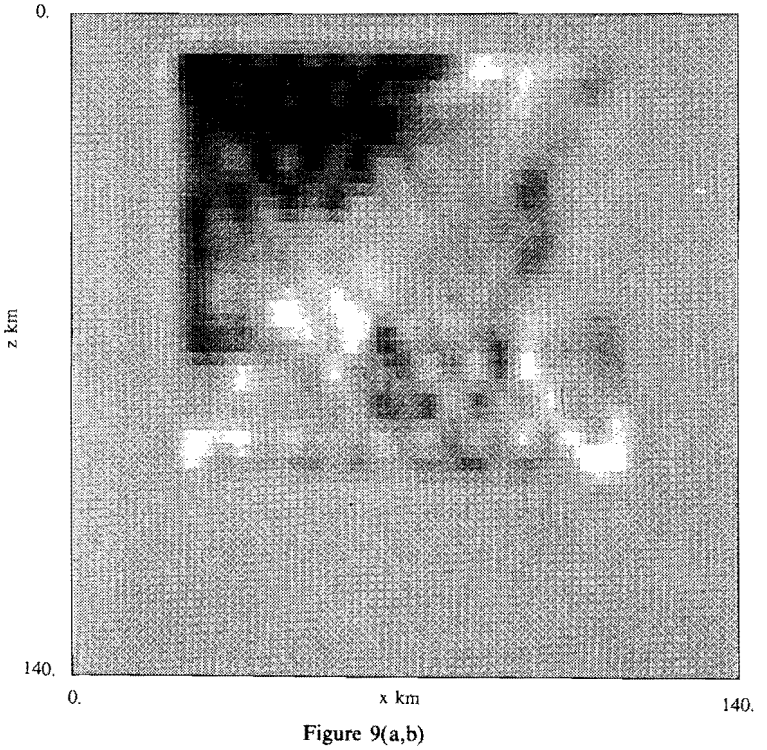

Figure 9(a,b)

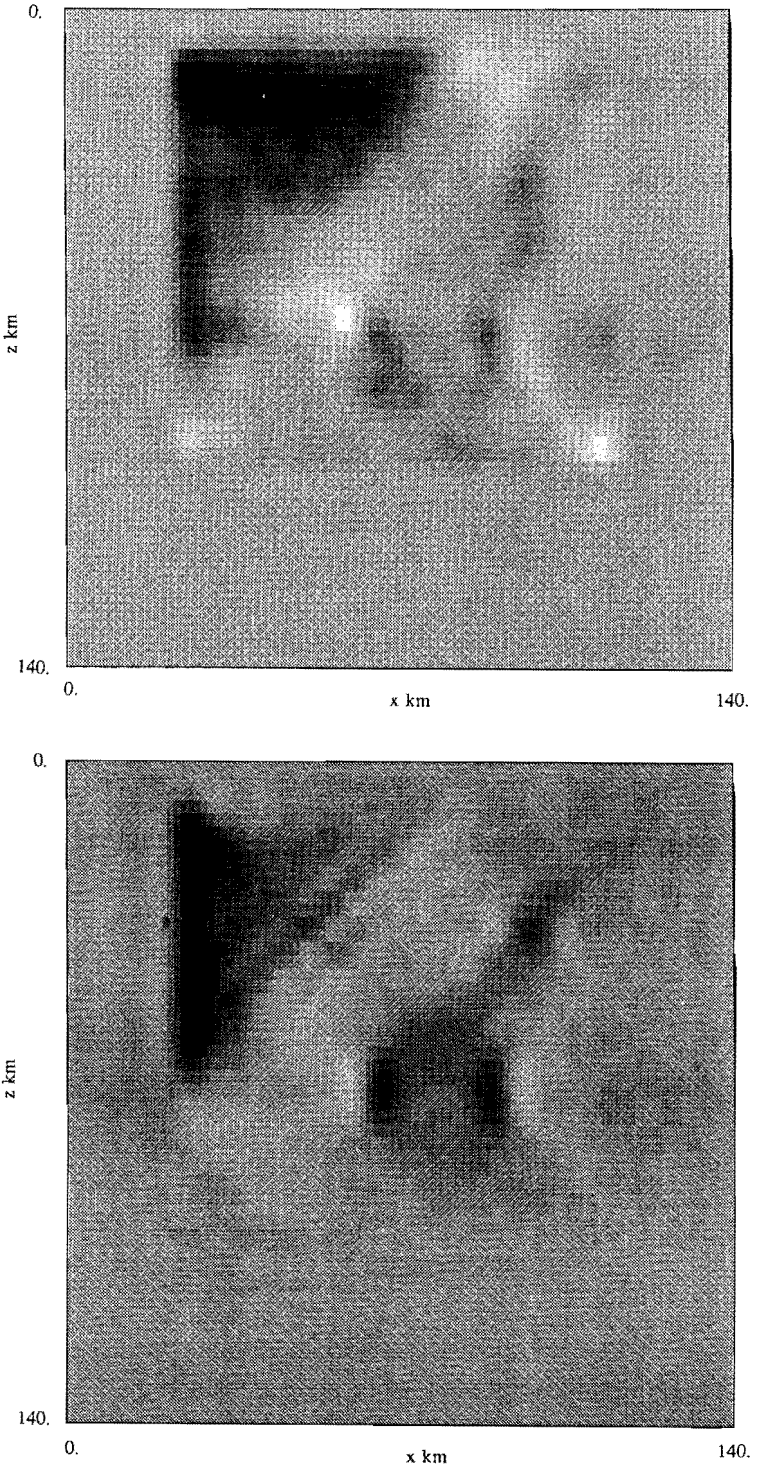

Figure 9(c,d)

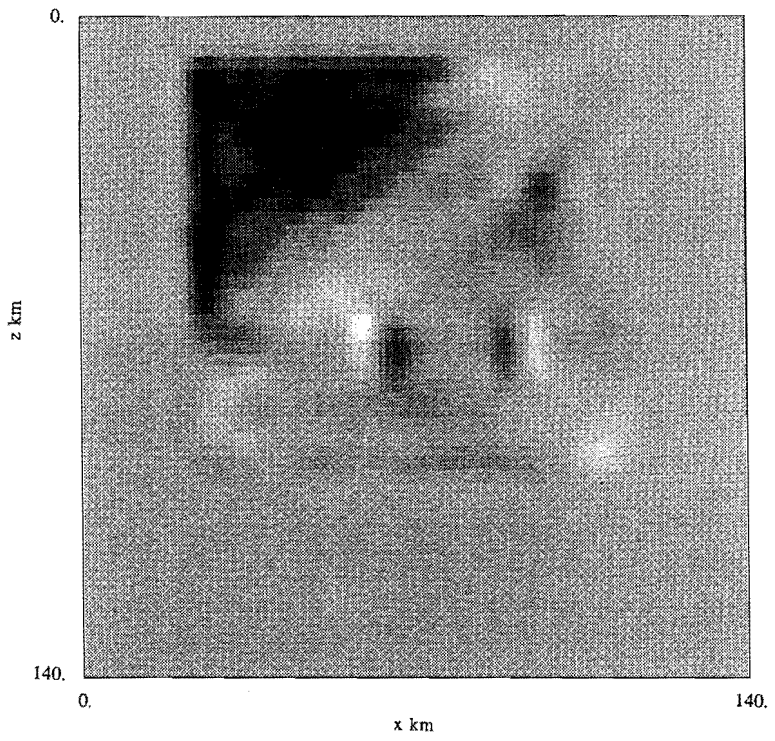

Figure 9

a) Trial model with several heterogeneities of different sizes with a contrast of 0.1 km/sec above a 6.0 km/sec background. Shading ranges from 5.95 to 6.14 km/sec. b) Travel time inversion with $\varepsilon_1 = 2$ and $\varepsilon_2 = 1$. Shading ranges from 5.96 to 6.12 km/sec for b), c), d) and e). c) Travel time inversion with $\varepsilon_1 = 5$ and $\varepsilon_2 = 2.5$. d) Amplitude inversion with $\varepsilon_1 = 4$ and $\varepsilon_2 = 2$. e) Combined travel time and amplitude inversion equally weighted with $\varepsilon_1 = 5$ and $\varepsilon_2 = 4$.

the heterogeneity quite sharply, but there is little solid fill, which the amplitude is less sensitive to. Also, since the top and bottom of the model are, in this ray geometry, sampled by nearly vertical rays, less of an amplitude signature comes from these. For a wider range of ray angles, the top and bottom of the mode would be better resolved. Nonetheless, solid fill would not be well reconstructed from the linearized amplitude inversion. By using a multiple step nonlinear inversion, possibly more of the solid fill of the anomaly could be reconstructed using the amplitudes.

The final model shown in Figure 9a has several heterogeneities of different sizes and shapes. The heterogeneities have 0.1 km/sec contrast above the 6.0 km/sec background. Sources are below and receivers are along the top surface. Figure 9b shows a travel time inversion using only a small amount of damping with $\varepsilon_1 = 2$ and $\varepsilon_2 = 1$. This results in a checker-board pattern of high and low velocities caused by the limited ray aperture. Figure 9c shows a travel time inversion using more

damping and smoothing with $\varepsilon_1 \approx \sigma_v^{-1} = 5$ and $\varepsilon_2 = 2.5$. This gives a much smoother result. Now the upper triangular heterogeneity is seen but the smaller heterogeneities are only suggested.

The same model is inverted using amplitude in Figure 9d. The damping and smoothing are $\varepsilon_1 = 4$ and $\varepsilon_2 = 2$. The vertical edges of all the heterogeneities are now seen. There is also a suggestion of the lower edge of the upper triangular body. But, horizontal edges and solid fill have not been recovered. More angular coverage would improve the horizontal interface but not the solid fill. In Figure 9e, a combined travel time and amplitude inversion is shown. The weighting between the normalized amplitude and travel time rows is one, and the damping and smoothing are $\varepsilon_1 = 5$ and $\varepsilon_2 = 4$. Both the solid fill and the edges of the triangular body are being reconstructed. Also, the smaller heterogeneities are clearly located.

4. Conclusions

Perturbation methods have been used to compute ray theoretical amplitudes and travel times in slightly perturbed velocity models. This approach results in a number of possible forward modeling applications. For example, ray theoretical solutions in complicated velocity models could be computed by perturbation analysis using ray tracing in nearby simpler models, such as 1-D models. Using the NORSAR model as an example, amplitudes were successfully computed by perturbation using a starting model up to 8% different from the final model. This approach can also be directly used for the calculation of Gaussian beam and Maslov synthetics seismograms in slightly perturbed velocity models. Also there may be applications of this approach for models with slight anisotropy, less than 10%, where all ray calculations could be done in nearby isotropic models.

For ray theoretical inversion problems, linear sensitivity operators for both travel time and amplitude have been efficiently calculated by perturbation analysis. The initial inversions used smaller variations of 1.7 percent to avoid possible problems with ray shift, however the perturbation approach is valid for larger variations. The results of trial inversions indicate that amplitude and travel time are sensitive to different features of the velocity models. Amplitudes appear to be more sensitive to the location of edges of velocity anomalies. Thus linearized inversions based on amplitudes are complementary and not redundant to travel time inversions, even in smoothly varying models. Further work should involve multiple step nonlinear inversions using travel times and amplitudes.

Acknowledgments

The authors wish to thank the reviewer for useful and constructive comments. This work was supported by NSF Grant No. EAR–8518147.

REFERENCES

AKI, K. (1977), *Three Dimensional Seismic Velocity Anomalies in the Lithosphere*, J. Geophys. *43*, 235–242.

AKI, K., CHRISTOFFERSSON, A., and HUSEBYE, E. S. (1976), *Determination of the Three-Dimensional Seismic Structure of the Lithosphere*, J. Geophys. Res. *82*, 277–296.

AKI, K. and RICHARDS, P., *Quantitative Seismology: Theory and Methods* (W.H. Freeman and Co., San Francisco, California 1980).

ČERVENÝ, V. (1985a), *The Application of Ray Tracing to the Numerical Modeling of Seismic Wavefields in Complex Structures*. In *Handbook of Geophysical Exploration, Section 1: Seismic Exploration* (Helbig, K. and Treitel, S., eds.), Volume 15A on Seismic Shear Waves, Dohr, G. ed.: 1–119, Geophysical Press, London.

ČERVENÝ, V. (1985b), *Gaussian Beam Synthetic Seismograms*, J. Geophys. *58*, 44–72.

ČERVENÝ, V. and FIRBAS, P. (1984), *Numerical Modelling and Inversion of Travel Time of Seismic Body Waves in Inhomogeneous Anisotropic Media*, Geophys. J. R. Astr. Soc. *76*, 41–51.

ČERVENÝ, V. and HRON, F. (1980), *The Ray Series Method and Dynamic Ray Tracing System for Three-Dimensional Inhomogeneous Media*, Bull. Seism. Soc. Am. *70*, 47–77.

ČERVENÝ, V., KLIMEŠ, L., and PŠENČÍK, I. (1984), *Paraxial Ray Approximations in the Computation of Seismic Wavefields in Inhomogeneous Media*, Geophys. J. R. Astr. Soc. *79*, 89–104.

ČERVENÝ, V., PLEINEROVA, J., KLIMEŠ, L., and PŠENČÍK, I. (1987), *High-Frequency Radiation from Earthquake Sources in Laterally Varying Layered Structures*, Geophys. J. R. Astr. Soc. *88*, 43–79.

ČERVENÝ, V., POPOV, M. M., and PŠENČÍK, I. (1982), *Computation of Wavefields in Inhomogeneous Media—Gaussian Beam Approach*, Geophys. J. R. Astr. Soc. *70*, 109–128.

ČERVENÝ, V. and PŠENČÍK, I. (1984), *Documentation of Earthquake Algorithms. SEIS83—Numerical Modeling of Seismic Wave Fields in 2-D Laterally Varying Layered Structures by the Ray Method.* 36-40, ed. Engdahl, E. R., Report SE-35, Boulder, Colorado.

CLAYTON, R. and COMER, R. (1983), *A Tomographic Analysis of Mantle Heterogeneities from Body Wave Travel Time Data (abstract)*, EOS Trans. AGU *64*, 776.

CORMIER and BEROZO (1987), *Calculation of Strong Ground Motion due to an Extended Earthquake Source in a Laterally Varying Structure*, Bull. Seism. Soc. Am. *77*, 1–14.

DZIEWONSKI, A. M. (1984), *Mapping the Lower Mantle: Determination of Lateral Heterogeneity in P-velocity up to Degree and Order 6*, J. Geophys. Res. *89*, 5929–5952.

FARRA, V. and MADARIAGA, R. (1987), *Seismic Waveform Modeling in Heterogeneous Media by Ray Perturbation Theory*, J. Geophys. Res. *92*, 2697–2712.

HADDON, R. A. W. and HUSEBYE, E. S. (1978), *Joint Interpretation of P-Wave Time and Amplitude Anomalies in Laterally Heterogeneous Media*, Geophys. J. R. Astr. Soc. *55*, 19–43.

LUENBERGER, D. G., *Introduction to Linear and Nonlinear Programming* (Addison-Wesley, Reading, Massachusetts 1984).

NOLET, G. (1985), *Solving of Resolving Inadequate and Noisy Tomographic System*, J. Comput. Phys. *61*,463–482.

NOWACK, R. L. and AKI, K. (1984), *The 2-D Gaussian Beam Synthetic Method: Testing and Application*, J. Geophys. Res. *89*, 7797–7819.

NOWACK, R. L. and AKI, K. (1986), *Iterative Inversion for Velocity Using Waveform Data*, Geophys. J. R. Astr. Soc. *87*, 701–730.

PAIGE, C. C. and SAUNDERS, M. A. (1982), *LSQR: An Algorithm for Sparse Linear Equations and Sparse Least Squares*, ACM Trans. Math. Software *8*, 43–71.

PAIGE, C. C. and SAUNDERS, M. A. (1982), *Algorithm 583—LSQR: Sparse Linear Equations and Least Squares Problems*, ACM Trans. Math. Software *8*, 195–209.

POPOV, M. M. and PŠENČÍK, I. (1976), *Ray Amplitudes in Inhomogeneous Media with Curved Interfaces*, Geofyzikalni Sbornik *24*, 111–129.

POPOV, M. M. and PŠENČÍK, I. (1978), *Computation of Ray Amplitudes in Inhomogeneous Media with Curved Interfaces*, Studia Geophys. et Geod. *22*, 248–258.

THOMSON, C. J. (1983), *Ray-Theoretical Amplitude Inversion for Laterally Varying Velocity Structure Below NORSAR*, Geophys. J. R. Astr. Soc. *74*, 525–558.

THOMSON, C. J. and GUBBINS, D. (1982), *Three-Dimensional Lithosphere Modeling at NORSAR: Linearity of the Method and Amplitude Variations of the Anomalies*, Geophys. J. R. Astr. Soc. *71*, 1–36.

(Received June 1, 1987, revised January 7, 1988, accepted January 14, 1988)